


^8He and ^9Li cluster structures in light nucleiNaoyuki Itagaki,¹ Tokuro Fukui,¹ Junki Tanaka ,² and Yuma Kikuchi³¹*Yukawa Institute for Theoretical Physics, Kyoto University, Kitashirakawa Oiwake-Cho, Kyoto 606-8502, Japan*²*RIKEN Nishina Center for Accelerator-Based Science, 2-1 Hirosawa, Wako, Saitama 351-0198, Japan*³*Tokuyama College of Technology, Gakuendai, Shunan, Yamaguchi 745-8585, Japan*

(Received 30 April 2020; revised 19 July 2020; accepted 17 August 2020; published 27 August 2020)

The possibility of the ^8He and ^9Li clusters in atomic nuclei is discussed. Until now most of the clusters in the conventional models have been limited to the closures of the three-dimensional harmonic oscillators, such as ^4He , ^{16}O , and ^{40}Ca . In the neutron-rich nuclei, however, the neutron-to-proton ratio (N/Z) is not unity, and it is worthwhile to think about more neutron-rich objects with $N > Z$ as the building blocks of cluster structures. Here the nuclei with the neutron number six, which is the subclosure of the $p_{3/2}$ subshell of the jj -coupling shell model, are assumed to be clusters, and thus we study the ^8He and ^9Li cluster structures in ^{16}Be ($^8\text{He} + ^8\text{He}$), ^{17}B ($^8\text{He} + ^9\text{Li}$), ^{18}C ($^9\text{Li} + ^9\text{Li}$), and ^{24}C ($^8\text{He} + ^8\text{He} + ^8\text{He}$). Recent progress of the antisymmetrized quasi-cluster model (AQCM) enables us to utilize jj -coupling shell-model wave functions as the clusters rather easily. It is shown that the $^8\text{He} + ^9\text{Li}$ and $^9\text{Li} + ^9\text{Li}$ cluster configurations cover the lowest shell-model states of ^{17}B and ^{18}C , respectively. To predict cluster states with large relative distances, we increase the expectation value of the principal quantum numbers by adding the nodes to the lowest states under the condition that the total angular momentum is unchanged (equal to $J^\pi = 0^+$). As a result, developed cluster states are obtained around the corresponding threshold energies. The rotational band structure of ^{24}C , which reflects the symmetry of equilateral triangular configuration (D_{3h} symmetry) of three ^8He clusters, also appears around the threshold energy. We suggest a novel mechanism whereby the spin-orbit interaction induces the clustering, which is distinctive of neutron-rich nuclei.

DOI: [10.1103/PhysRevC.102.024332](https://doi.org/10.1103/PhysRevC.102.024332)**I. INTRODUCTION**

^4He nuclei have been known as α clusters, which can be subsystems in some light nuclei [1,2]. The binding energy of ^4He is quite large in the light-mass region, and, on the contrary, the relative interaction between ^4He nuclei is weak. Therefore, each ^4He can be considered as a subunit called an α cluster. The candidates for α cluster structures have been discussed for many years [3], including the second 0^+ state of ^{12}C with a developed three- α cluster structure called a Hoyle state [4].

In most conventional cluster models, the clusters have been limited to the closure of the three-dimensional harmonic oscillator, such as ^4He , ^{16}O , and ^{40}Ca , where the contribution of the noncentral interactions (spin-orbit and tensor interactions) vanishes. However, in the nuclear systems, the symmetry of the jj -coupling shell model is more important, where the contribution of the spin-orbit interaction breaks the symmetry of the three-dimensional harmonic oscillator, and the subclosure of j -upper shells, $f_{7/2}$, $g_{9/2}$, and $h_{11/2}$, is essential in explaining the observed magic numbers of 28, 50, and 126 [5]. Indeed, this spin-orbit interaction is also known as a driving force in breaking the α clusters [6]. Therefore, it would be meaningful to extend the traditional definition of the clusters; different objects could be candidates for the clusters.

Now we focus on neutron-rich nuclei, which have been the main subject of nuclear structure physics for decades. In neutron-rich nuclei, the ratio of proton number and neutron number deviates from unity. Therefore, it is worthwhile to consider neutron-rich clusters whose neutron numbers correspond to the subclosure of the j -upper orbits of the jj -coupling shell model, where the spin-orbit interaction works attractively. Here we discuss the possibility that nuclei with the neutron number six, which is the subclosure of the j -upper shell, $p_{3/2}$, can be clusters. Previously we have discussed the possibility of the ^{14}C cluster as the building block of medium-heavy nuclei [7], whose proton number (six) corresponds to the subclosure of $p_{3/2}$. As the next step, we show the possibility of the ^8He (two protons and six neutrons) and ^9Li (three protons and six neutrons) cluster structures in ^{16}Be ($^8\text{He} + ^8\text{He}$), ^{17}B ($^8\text{He} + ^9\text{Li}$), ^{18}C ($^9\text{Li} + ^9\text{Li}$), and ^{24}C ($^8\text{He} + ^8\text{He} + ^8\text{He}$).

It has been reported that Be isotopes are well described as two α clusters with valence neutrons. Here, the molecular-orbit structure of the valence neutrons, where each valence neutron rotates not around only one α cluster but around two α clusters, has been found to be important [8–14]. Thus, $^4\text{He} + ^6\text{He}$ and $^5\text{He} + ^5\text{He}$ configurations mix, for instance, in ^{10}Be . However, it is also known that some of the excited states of ^{12}Be has not the molecular-orbit but the atomic-orbit structure of the $^6\text{He} + ^6\text{He}$ or $^4\text{He} + ^8\text{He}$ configuration [13,15,16],

where each valence neutron sticks to one of the α clusters. It should be stressed that the appearance of both molecular- and atomic-orbit structures in Be isotopes, including ^{16}Be , has been systematically studied with the generalized two-center cluster model (GTCM) [17]. In the present study, we treat ^8He as a cluster based on the atomic-orbit picture and go beyond the Be isotopes.

The nucleus ^8He is located at the dripline of the He isotopes and has a neutron-halo structure. The valence neutrons are known to have an intermediate character of a di-neutron structure and independent particle motion [18,19]. Nevertheless, the two-neutron separation energy of 2.12 MeV is larger than that of ^6He (0.98 MeV), and here we simplify it with the jj -coupling shell-model configuration with the ^4He core and consider this nucleus as a subunit.

We also introduce the ^9Li cluster and discuss ^{17}B ($^8\text{He} + ^9\text{Li}$) and ^{18}C ($^9\text{Li} + ^9\text{Li}$). The neutron separation energy of ^9Li is 4.06 MeV and not very large, but this is larger than that of ^8He and various $^9\text{Li} + n + n$ models have been applied to ^{11}Li so far [20]. Although the structure of ^9Li itself is a subject to be carefully investigated, here we simplify it as a cluster by using the lowest shell-model configuration, as in the ^8He case, and discuss the cluster structure in the heavy nuclei. The two-center-like deformation was predicted in ^{17}B with the $^8\text{He} + ^9\text{Li}$ configuration [21], and we further investigate the appearance of more developed cluster states around the threshold energy.

The neutron-rich clusters introduced in this article have smaller binding energies compared with those of traditional cluster models. However, the final goal of the present study is to verify how weakly bound neutrons around these “newly defined” clusters stabilize the binding of the molecular states. For instance, one of the targets is the $^9\text{Li} + ^9\text{Li} + n + n$ configuration of ^{20}C around the four-body threshold. The ^{11}Li nucleus is the famous halo-nucleus, and how two ^9Li clusters share the two weakly bound neutrons around the threshold energy is an intriguing question. The ^8He and ^9Li clusters are considered to be well bound compared with these weakly bound valence neutrons and could be treated as clusters. In the present article, the weakly-bound valence neutrons are not yet added and the main focus is on the cluster structure of the core part ($^8\text{He} + ^9\text{Li}$ and $^9\text{Li} + ^9\text{Li}$), but this is the important first step.

Recently, the wave functions of the jj -coupling shell model were easily prepared by starting from the cluster model. Indeed, the antisymmetrized quasi-cluster model (AQCM) proposed in Refs. [7,22–32] allows for a smooth transformation of the cluster model wave functions to the jj -coupling shell-model wave functions, as well as the incorporation of the effects of the spin-orbit interaction, which is absent in many of the traditional α cluster models. Therefore, now we can utilize jj -coupling shell-model wave functions as the building blocks of the cluster structure. In this article, we introduce ^8He and ^9Li clusters by using the AQCM.

In this paper, we discuss how the $^8\text{He} + ^9\text{Li}$ and $^9\text{Li} + ^9\text{Li}$ cluster configurations cover the lowest shell-model states of ^{17}B and ^{18}C , respectively. Also, we show the appearance of developed cluster states around the corresponding threshold energies by orthogonalizing them to the lowest states. In

addition, the rotational band structure of ^{24}C , which reflects the symmetry of the equilateral triangular configuration (D_{3h} symmetry) of three ^8He clusters, will be presented. Although these cluster states are above the neutron-threshold energies, they appear around the cluster-threshold energies.

This paper is organized as follows: The framework of AQCM is described in Sec. II. The results are shown in Sec. III, where the $^8\text{He} + ^8\text{He}$ structure in ^{16}Be , the $^9\text{Li} + ^8\text{He}$ structure in ^{17}B , the $^9\text{Li} + ^9\text{Li}$ structure in ^{18}C , and the three ^8He structure in ^{24}C are discussed in Secs. III A–III D, respectively. The conclusions are presented in Sec. IV.

II. FRAMEWORK

A. Wave function

We analyze the ^8He and ^9Li cluster structures within the framework of the AQCM. The neutrons of these clusters correspond to the subclosure of $p_{3/2}$ in the jj -coupling shell model, which can be easily prepared starting from the cluster model; the AQCM allows for the smooth transformation of the cluster model wave functions to the jj -coupling shell-model wave functions.

In the AQCM, each single particle is described by a Gaussian form, as in many other cluster models, including the Brink model [1],

$$\phi = \left(\frac{2\nu}{\pi}\right)^{\frac{3}{4}} \exp[-\nu(\mathbf{r} - \boldsymbol{\zeta})^2] \chi, \quad (1)$$

where the Gaussian center parameter $\boldsymbol{\zeta}$ is related to the expectation value of the position of the nucleon, and χ is the spin-isospin part of the wave function. For the size parameter ν , we use $\nu = 0.23 \text{ fm}^{-2}$.

The Slater determinant Φ_{SD} is constructed from these single-particle wave functions by antisymmetrizing them, and then Φ_{SD} is projected onto the eigenstates of the angular momenta by numerical integration,

$$\Phi_{MK}^J = \frac{2J+1}{8\pi^2} \int d\Omega D_{MK}^J{}^* R(\Omega) \Phi_{\text{SD}}. \quad (2)$$

Here D_{MK}^J is the Wigner D function and $R(\Omega)$ is the rotation operator for the spatial and spin parts of the wave function. This integration over the Euler angle Ω is numerically performed.

Next we focus on the Gaussian center parameters $\{\boldsymbol{\zeta}\}$. As in other cluster models, here four single-particle wave functions with different spin and isospin sharing a common $\boldsymbol{\zeta}$ value correspond to an α cluster. This cluster wave function is transformed to jj -coupling shell model based on the AQCM. When the original value of the Gaussian center parameter $\boldsymbol{\zeta}$ is \mathbf{R} , which is real and related to the spatial position of this nucleon, it is transformed by adding the imaginary part as

$$\boldsymbol{\zeta} = \mathbf{R} + i\Lambda \mathbf{e}^{\text{spin}} \times \mathbf{R}, \quad (3)$$

where \mathbf{e}^{spin} is a unit vector for the intrinsic-spin orientation of this nucleon. The control parameter Λ is associated with the breaking of the cluster and with a finite value of Λ , the two nucleons with opposite spin orientations have the $\boldsymbol{\zeta}$ values,

which are complex conjugates of each other. This situation corresponds to the time-reversal motion of two nucleons.

Here we explain the intuitive meaning of this procedure. The inclusion of the imaginary part allows us to directly connect the single-particle wave function to the spherical harmonics of the jj -coupling shell model. Suppose that the Gaussian center parameter ζ has the x component, and the spin direction is defined along the z axis (this is the spin-up nucleon). According to Eq. (3), the imaginary part of ζ is given to its y component. Then we think about the cross term of the exponent in Eq. (1), $\exp[2\nu\zeta \cdot \mathbf{r}]$. After the Taylor expansion, the p -wave component is proportional to $\zeta \cdot \mathbf{r} \propto (x + i\Delta y)$. At $\Lambda = 1$, this is proportional to Y_{11} of the spherical harmonics. The nucleon is spin-up, and thus the coupling with the spin part gives the stretched state of the angular momentum, $|3/2 \ 3/2\rangle$ of the jj -coupling shell model, where the spin-orbit interaction acts attractively. For the spin-down nucleon, we introduce the complex conjugate ζ value, which gives $|3/2 \ -3/2\rangle$. The next two nucleons are generated by rotating the ζ values and spin-directions of these two nucleons by $2\pi/3$. The last two nucleons are generated by changing the rotation angle to $4\pi/3$. Eventually, all six nucleons have spin-stretched states and, after the antisymmetrization, the configuration becomes the subclosure configuration of $(s1/2)^2(p3/2)^4$. The details are shown in Ref. [27].

For the description of ⁸He, at first, di-nucleon clusters are prepared; in each di-nucleon cluster, two nucleons with opposite spin and the same isospin share a common value for the Gaussian center parameters. For the proton part, one di-proton cluster is placed at the origin, which corresponds to the lowest $(0s)^2$ configuration of the shell model. For the neutron part, three di-neutron clusters are introduced with an equilateral triangular configuration and a small distance R between them, and the imaginary parts of the Gaussian center parameters are given by setting $\Lambda = 1$ in Eq. (3), which corresponds to the subclosure of the $p_{3/2}$ shell [22,27]. In the actual calculations, R is set to 0.1 fm. This ⁸He cluster is the eigenstate of $J^\pi = 0^+$, and projection of the total angular momentum of the total system just gives the orbital angular momentum of the relative motion in the case of ¹⁶Be (⁸He - ⁸He).

For ⁹Li, one more proton in the $p_{3/2}$ orbit is added. The Gaussian center parameter of the proton in the $p_{3/2}$ orbit is introduced in the following way: The proton is placed with a small x component ($R = 0.1$ fm), and the y component is given following Eq. (3), where the spin orientation is defined along the z axis (corresponding to a spin-up or spin-down proton). This ⁹Li cluster is the eigenstate of $J^\pi = 3/2^-$.

For the calculations of ¹⁶Be, ¹⁷B, and ¹⁸C, we translationally shift the Gaussian center parameters of the ⁸He and ⁹Li clusters and place them on the z axis. For ²⁴C, three ⁸He clusters are placed to have an equilateral triangular shape.

B. Hamiltonian

The Hamiltonian consists of the kinetic-energy and potential-energy terms. The potential energy has central (\hat{V}_{central}), spin-orbit ($\hat{V}_{\text{spin-orbit}}$), and Coulomb parts. For the

central part, the Tohsaki interaction (F1 parameter set) [33] is adopted, which has finite-range three-body nucleon-nucleon interaction terms in addition to two-body terms. This interaction is designed to reproduce both the saturation properties and scattering phase shifts of two α clusters. For the spin-orbit part, that of the G3RS interaction [34], which is a realistic interaction originally developed to reproduce the nucleon-nucleon scattering phase shifts, is adopted. The combination of these central and spin-orbit interactions has been investigated in detail in Refs. [31,32].

The Tohsaki interaction for the central part consists of two-body ($V^{(2)}$) and three-body ($V^{(3)}$) terms:

$$\hat{V}_{\text{central}} = \frac{1}{2} \sum_{i \neq j} V_{ij}^{(2)} + \frac{1}{6} \sum_{i \neq j, j \neq k, i \neq k} V_{ijk}^{(3)}, \quad (4)$$

where $V_{ij}^{(2)}$ and $V_{ijk}^{(3)}$ have three ranges,

$$V_{ij}^{(2)} = \sum_{\alpha=1}^3 V_{\alpha}^{(2)} \exp \left[-(\bar{r}_i - \bar{r}_j)^2 / \mu_{\alpha}^2 \right] (W_{\alpha}^{(2)} + M_{\alpha}^{(2)} P^r)_{ij}, \quad (5)$$

$$V_{ijk}^{(3)} = \sum_{\alpha=1}^3 V_{\alpha}^{(3)} \exp \left[-(\bar{r}_i - \bar{r}_j)^2 / \mu_{\alpha}^2 - (\bar{r}_i - \bar{r}_k)^2 / \mu_{\alpha}^2 \right] \times (W_{\alpha}^{(3)} + M_{\alpha}^{(3)} P^r)_{ij} (W_{\alpha}^{(3)} + M_{\alpha}^{(3)} P^r)_{ik}. \quad (6)$$

Here, P^r represents the exchange of the spatial part of the wave functions of two interacting nucleons. The position of the i th nucleon is expressed by \bar{r}_i . The details of the parameters are shown in Ref. [33].

The G3RS interaction is a realistic interaction, and the spin-orbit part has the following form:

$$\hat{V}_{\text{spin-orbit}} = \frac{1}{2} \sum_{i \neq j} V_{ij}^{ls}, \quad (7)$$

$$V_{ij}^{ls} = (V_{ls}^1 e^{-d_1(\bar{r}_i - \bar{r}_j)^2} - V_{ls}^2 e^{-d_2(\bar{r}_i - \bar{r}_j)^2}) P(^3O) \vec{L} \cdot \vec{S}. \quad (8)$$

We use the original ‘‘case 1’’ values shown in Ref. [34] for the range and the strength of the spin-orbit interaction. Here \vec{L} is the angular momentum for the relative motion between the i th and j th nucleons, and \vec{S} is the sum of the spin operator for these two interacting nucleons. The operator $P(^3O)$ stands for the projection onto the triplet-odd state.

III. RESULTS

A. ⁸He + ⁸He cluster structure in ¹⁶Be

We start the discussion with the ⁸He + ⁸He cluster structure in ¹⁶Be. The dripline nucleus of the Be isotopes is ¹⁴Be, and thus ¹⁶Be is located outside the neutron dripline. Experimentally, the two-neutron separation energy is -1.35 MeV (unbound), but the ground state is lower than the ⁸He + ⁸He threshold by 5.77 MeV.

First, we show that the ⁸He + ⁸He model space covers the lowest principal quantum number of ¹⁶Be. The expectation value for the principal quantum number n of the harmonic oscillator for the 0^+ state of ¹⁶Be is shown in Fig. 1 as a function of the distance between two ⁸He clusters. The dotted

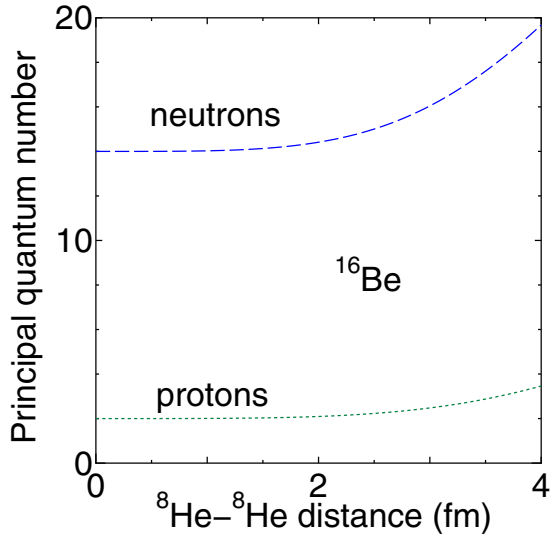


FIG. 1. Expectation value for the principal quantum number of the harmonic oscillator (n) for the 0^+ state of ^{16}Be as a function of the distance between two ^8He clusters. Dotted and dashed lines are results for the protons and neutrons, respectively.

and dashed lines represent the results for the protons and neutrons, respectively, which converge to 2 and 14 at small relative distances. These values agree with those for the lowest shell-model configuration; for the protons, two are in the lowest $0s$ shell and two are in the p shell ($2 \times 1 = 2$), and, for the neutrons, two are in the lowest $0s$ shell, six are in the p shell, and four are in the sd shell ($6 \times 1 + 4 \times 2 = 14$). Hence, the lowest shell-model configuration is included in the model space. Upon increasing the relative distance between the two ^8He clusters, the components of higher shells mix, and the n value rapidly increases.

Next, the energy curves for ^{16}Be measured from the two- ^8He threshold is shown in Fig. 2 as a function of the distance between two ^8He clusters. The solid, dotted, and dashed lines are the results for the 0^+ , 2^+ , and 4^+ states, respectively. It can be seen that the optimal energy for the 0^+ state is obtained with the relative distance of ≈ 3 fm. This means that the lowest energy is not obtained at the limit of the shell model, and clustering is found to be important, which is indeed higher shell mixing in terms of the shell model. Although we do not have adjustable parameters, the lowest energy is close to the experimental binding energy of 5.77 MeV. Despite this binding energy, which is sufficiently large, the optimal distance is large owing to the Pauli-blocking effect at short relative distances between the two ^8He clusters, and developed cluster structure appears. For the 2^+ and 4^+ states, the optimal distances are slightly larger than that for the 0^+ state due to the centrifugal force.

B. $^9\text{Li} + ^8\text{He}$ cluster structure in ^{17}B

We add one proton and show the result of $^9\text{Li} - ^8\text{He}$ cluster configuration in ^{17}B . The dashed line in Fig. 3 shows the energy for the lowest $3/2^-$ state of ^{17}B measured from the $^9\text{Li} - ^8\text{He}$ threshold as a function of the distance between ^9Li

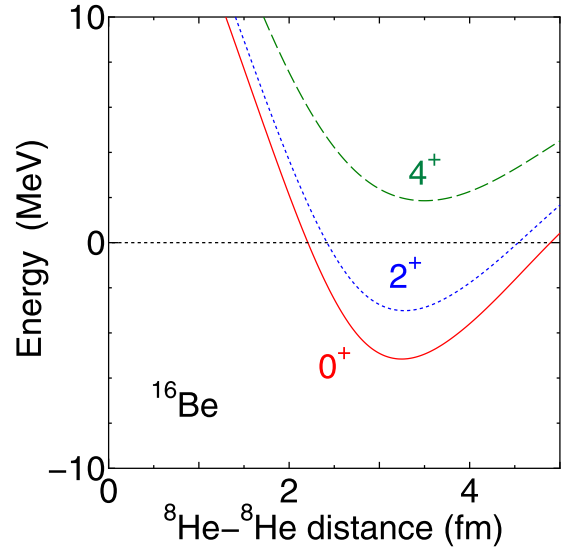


FIG. 2. Energy curves for ^{16}Be measured from the two- ^8He threshold as a function of the distance between two ^8He clusters. Solid, dotted, and dashed lines correspond to the 0^+ , 2^+ , and 4^+ states, respectively.

and ^8He . Experimentally, the ^{17}B nucleus is bound from the $^9\text{Li} + ^8\text{He}$ threshold by 12.86 MeV. It is not perfect, but the lowest energy obtained is fairly close to this value. Similarly to the $^8\text{He} + ^8\text{He}$ case, despite this large binding energy, the relative distance at the optimal energy is also large owing to the Pauli-blocking effect at short relative distances between the two clusters. In this calculation, ^9Li and ^8He clusters are placed on the z axis, while the last proton in ^9Li stays on the perpendicular plane, and there is no additional excitation to higher shells for this proton when the ^8He cluster approaches.

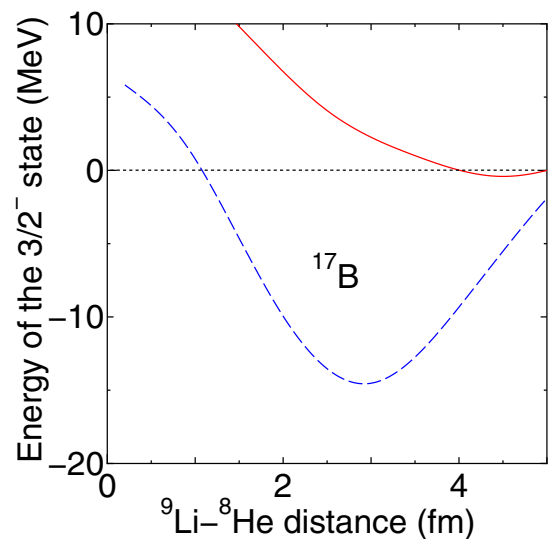


FIG. 3. Energy for the $3/2^-$ state of ^{17}B measured from the $^9\text{Li} - ^8\text{He}$ threshold as a function of the distance between ^9Li and ^8He (dashed line). Energy curve for the $3/2^-$ state orthogonal to the state having the optimal distance of 3 fm (solid line).

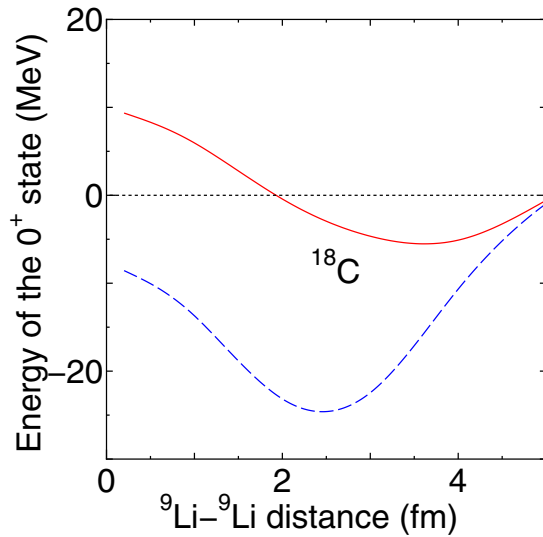


FIG. 4. Energy for the 0^+ state of ^{18}C measured from the two- ^9Li threshold as a function of the distance between two ^9Li clusters (dashed line). Energy curve for the 0^+ state orthogonal to the state having the optimal distance of 2.5 fm (solid line).

Therefore, again the lowest principal quantum number of ^{17}B is included in the model space.

The energy curve for the $3/2^-$ state orthogonal to the lowest state (relative distance of 3 fm) is shown as the solid line. It is intriguing to see that the energy minimum point appears around the threshold energy with a very large relative distance of 4 fm. The appearance of very developed cluster structure around the threshold is expected, and adding neutrons to this state and investigating the molecular-orbital structure will be performed in the near future.

C. $^9\text{Li} + ^9\text{Li}$ cluster structure in ^{18}C

For ^{18}C , we introduce a $^9\text{Li} + ^9\text{Li}$ model. Here the spin directions of the valence protons in two ^9Li clusters are

introduced to be antiparallel, and two valence protons occupy the time-reversal orbits. Thus again the model space covers the lowest principal quantum number of ^{18}C . The dashed line in Fig. 4 shows the energy for the lowest 0^+ state of ^{18}C measured from the two- ^9Li threshold as a function of the distance between two ^9Li clusters. The optimal energy is obtained around the relative distance of 2.5 fm. Experimentally, the ground state of ^{18}C is lower than the two- ^9Li threshold by 24.99 MeV. Again, although we do not use any adjustable parameter, the obtained optimal energy is fairly close to this value.

The solid line in Fig. 4 shows the energy curve for the 0^+ state orthogonal to the lowest state with the relative distance of 2.5 fm. Again, the appearance of the significantly clustered state around the threshold energy with the relative distance of ≈ 4 fm is expected. The intrinsic densities of this state on the xz plane ($y = 0$) with the relative distance of 4 fm are represented by Figs. 5(a) and 5(b) for protons and neutrons, respectively. As a future work, adding neutrons to this state would be interesting.

D. Three ^8He cluster structure in ^{24}C

Finally, we discuss the three ^8He cluster structure in ^{24}C . The dripline nucleus of the C isotopes is ^{22}C and hence ^{24}C is beyond the neutron dripline. Nevertheless, the three- ^8He states are shown to appear around the threshold energy. First, we show that the three ^8He configuration with the equilateral triangular configuration covers the lowest principal quantum number of the shell model. The expectation value for the principal quantum number of the harmonic oscillator for the 0^+ state of ^{24}C with the equilateral triangular configuration of three ^8He clusters is shown in Fig. 6 as a function of the distance between two ^8He clusters. Here the dotted and dashed lines represent the results for the protons and neutrons, respectively. They converge to 4 and 26 at small relative distances, respectively. These values are ones for the lowest shell-model configuration; for the protons, two are in the lowest $0s$ shell and four are in the p shell ($4 \times 1 = 4$), and

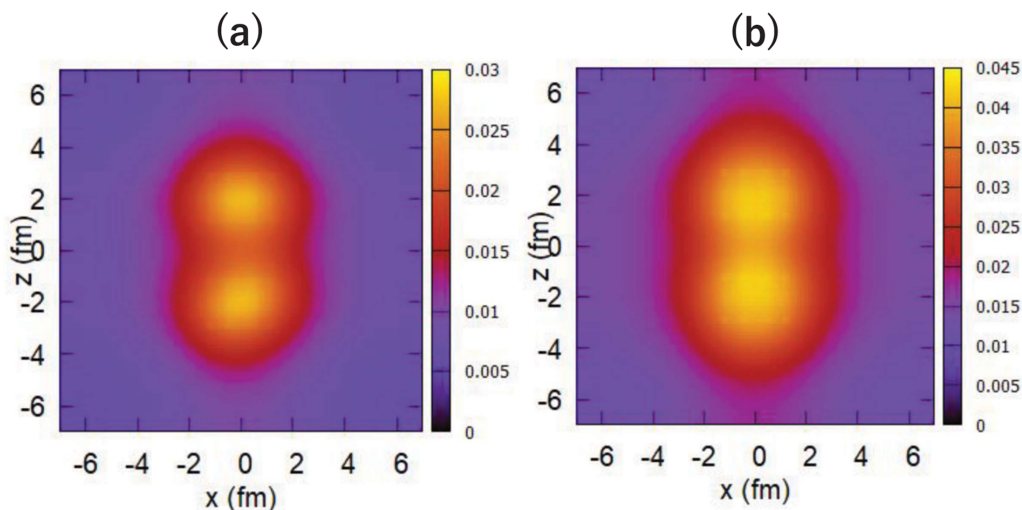


FIG. 5. Intrinsic density of $^9\text{Li} - ^9\text{Li}$ with the relative distance of 4 fm on the xz plane (fm^{-3}): (a) protons, (b) neutrons.

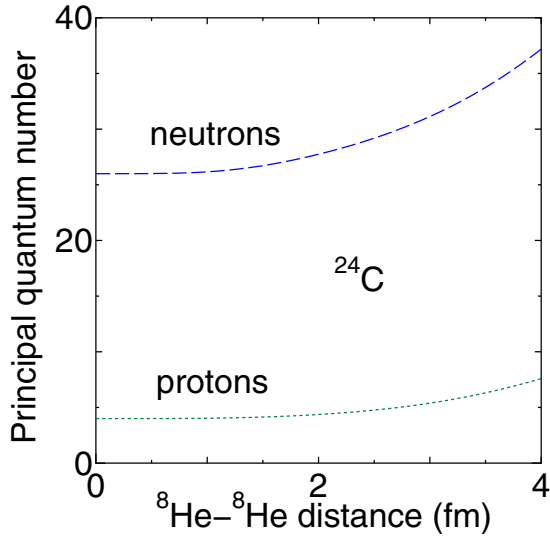


FIG. 6. Expectation value for the principal quantum number of the harmonic oscillator for the 0^+ state of ^{24}C with the equilateral triangular configuration of three ^8He clusters as a function of the distance between two ^8He clusters. Dotted and dashed lines correspond to the result for the protons and neutrons, respectively.

for the neutrons, two are in the lowest $0s$ shell, six are in the p shell, and ten are in the sd shell ($6 \times 1 + 10 \times 2 = 26$). Therefore, surprisingly enough, the lowest principal quantum number of ^{24}C is included within the three- ^8He model with an equilateral triangular configuration. However, experimentally, the three- ^8He threshold is located quite high (more than $E_x = 25$ MeV) in the excitation energy, and thus the three- ^8He configuration corresponds to a highly excited state.

In Fig. 7, the energy curves of ^{24}C with the equilateral triangular configuration of three ^8He clusters measured from the three- ^8He threshold are shown as a function of the distance between two ^8He clusters. Here Fig. 7(a) displays the result for the positive-parity states with $K = 0$ (0^+ , 2^+ , and 4^+), and those for the negative-parity states with $K = 3$ (3^- , 4^- , and 5^-) can be found in Fig. 7(b). We can see that both bands appear around the three- ^8He threshold energy with large relative distance.

It sounds contradictory that, even if the three- ^8He model covers the lowest principal quantum number state of ^{24}C , the three- ^8He cluster configuration has the lowest energy around the three- ^8He threshold located quite high in the excitation energy of ^{24}C . This puzzle is interpreted as the spin-orbit effect. Although the three ^8He clusters can have the lowest principal quantum number of the shell model, the spin configuration is not necessarily associated with the lowest jj -coupling shell-model state; the spin configuration of the neutrons is designed to reproduce the subclosure configuration of $p_{3/2}$ in each ^8He (for the description of the ground state, we have to change the spin orientations). As a result, the energy goes up when three ^8He clusters approach in spite of a decrease of the principal quantum number to the lowest shell-model value. This tendency is confirmed in Fig. 8, which shows the spin-orbit energy for the 0^+ state of ^{24}C with the equilateral triangular configuration of three ^8He clusters as a function

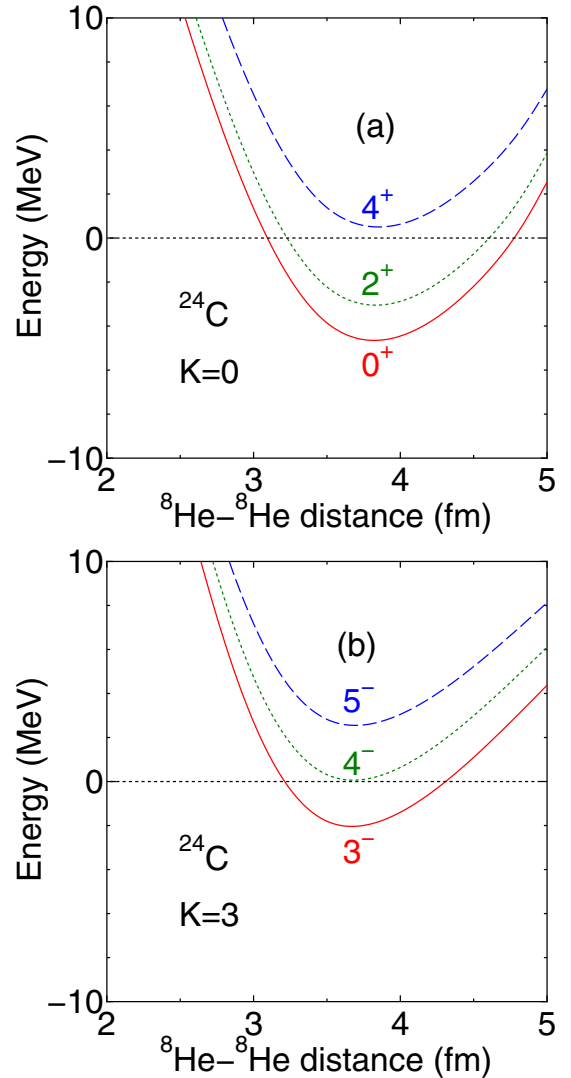


FIG. 7. Energy curves of ^{24}C with the equilateral triangular configuration of three ^8He clusters measured from the three- ^8He threshold as a function of the distance between two ^8He clusters. (a) Positive-parity $K = 0$ band, 0^+ , 2^+ , and 4^+ , and (b) negative-parity $K = 3$ band, 3^- , 4^- , and 5^- .

of the ^8He - ^8He distance. The spin-orbit interaction is the origin of the barrier at smaller relative distances. On the other hand, upon increasing the relative distance, the spin-orbit energy converges to the dotted line at -32.0 MeV, which shows the value three times the contribution in a free ^8He cluster. This barrier effect at short relative distances due to the spin-orbit interaction only occurs in the three ^8He -cluster case of ^{24}C and not in the binary cluster cases of ^{16}Be , ^{17}B , and ^{18}C . It becomes important with increasing number of clusters.

It has been known that, if the system has the equilateral triangular configuration (D_{3h} symmetry), both $K = 0$ (0^+ , 2^+ , 4^+ , ...) and $K = 3$ (3^- , 4^- , 5^- , ...) rotational bands are possible. The appearance of these rotational bands has been extensively discussed in ^{12}C [35], which is the signature of the equilateral triangular symmetry of the three α

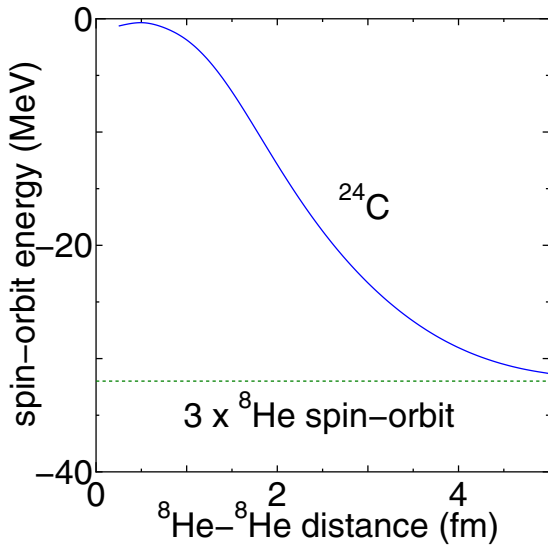


FIG. 8. The spin-orbit energy for the 0^+ state of ^{24}C with the equilateral triangular configuration of three ^8He clusters as a function of the ^8He - ^8He distance. The dotted line at -32.0 MeV shows the spin-orbit energy three times the contribution in a free ^8He cluster.

clusters. Now the α clusters are replaced with the ^8He clusters and what we discuss here is considered to be the neutron-rich version of the D_{3h} symmetry.

The energy eigenstates of the three- ^8He cluster states are obtained by superposing the Slater determinants with different relative distances and diagonalizing the Hamiltonian based on the generator coordinate method (GCM). The rotational band structure of the three- ^8He configuration is shown in Fig. 9, where the solid and dashed lines correspond to the result for $K = 0$ (positive parity, $0^+, 2^+, 4^+, \dots$) and $K = 3$ (negative

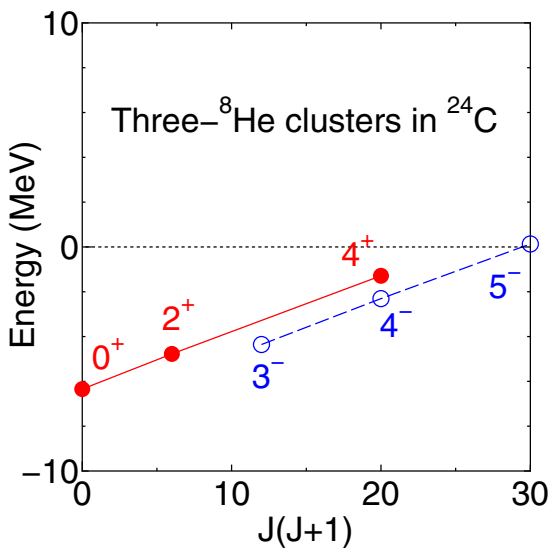


FIG. 9. Rotational band structure of three- ^8He configuration. Solid and dashed lines are the results for the $K = 0$ (positive parity, $0^+, 2^+, 4^+, \dots$) and $K = 3$ (negative parity, $3^-, 4^-, 5^-, \dots$) bands, respectively.

parity, $3^-, 4^-, 5^-, \dots$) bands, respectively. Two rotational band structures appear around the threshold energy and they have similar slopes as a function of $J(J + 1)$.

IV. CONCLUSIONS

Most of the conventional clusters so far investigated have been limited to the closure of the three-dimensional harmonic oscillator, such as ^4He , ^{16}O , and ^{40}Ca . Here we discussed the possibility that nuclei with the neutron number six, which is the subclosure of the $p_{3/2}$ subshell of the jj -coupling shell model, can be clusters; the ^8He and ^9Li cluster structures have been investigated in ^{16}Be ($^8\text{He} + ^8\text{He}$), ^{17}B ($^8\text{He} + ^9\text{Li}$), ^{18}C ($^9\text{Li} + ^9\text{Li}$), and ^{24}C ($^8\text{He} + ^8\text{He} + ^8\text{He}$).

We have shown that the lowest principal quantum numbers of ^{16}Be , ^{17}B , ^{18}C , and ^{24}C can be covered within this model. We have just adopted Tohsaki interaction, which has finite-range three-body terms, and there is no adjustable parameter in the Hamiltonian. Nevertheless the optimal energies of these nuclei measured from the corresponding threshold energies are fairly close to the experimental values. By orthogonalizing the wave functions to the lowest states, very developed cluster states were obtained around the corresponding threshold energies in ^{17}B and ^{18}C .

The appearance of $K = 0$ ($0^+, 2^+, 4^+, \dots$) and $K = 3$ ($3^-, 4^-, 5^-, \dots$) rotational bands has been extensively discussed in ^{12}C [35], which is the proof for the equilateral triangular symmetry of the three α clusters. In this study, we have replaced the α clusters with the ^8He clusters and shown the neutron-rich version of the rotational band structures for the configuration reflecting D_{3h} symmetry. The energy eigenstates of the three- ^8He cluster states are obtained by superposing the Slater determinants with different relative distances and diagonalizing the Hamiltonian. The two rotational band structures of the three- ^8He configuration appear around the threshold energy and have similar slopes as a function of $J(J + 1)$.

It is found that, although the three- ^8He cluster model covers the lowest principal quantum number of ^{24}C at short relative distances between clusters, the spin configuration of the neutrons is designed to reproduce the subclosure configuration of $p_{3/2}$ in each ^8He and is not necessarily associated with the ground state of ^{24}C . As a result, the energy goes up when three ^8He clusters approach, and the spin-orbit interaction works as a barrier for the smaller relative distances.

This is a novel mechanism for the clustering. Until now, in most of the conventional cluster models, clusters were spin-zero systems and the contribution of the spin-orbit interaction vanished after assuming these clusters. In addition, the spin-orbit interaction was considered to be the driving force, which breaks these clusters and promotes the symmetry of the jj -coupling shell model [6]. However, here we learn that, if we define jj -coupling shell-model wave functions as the “new” clusters, a completely opposite role of the spin-orbit interaction can be seen; the spin-orbit interaction induces the clustering when it acts attractively in each cluster. This barrier effect at short relative distances due to the spin-orbit interaction cannot be seen in the binary cluster cases of ^{16}Be , ^{17}B , and ^{18}C . It becomes evident with increasing number of clusters, as in the three ^8He -cluster case of ^{24}C .

As future work, the appearance of the molecular-orbital structure will be studied by adding neutrons to the developed cluster states obtained here in ^{17}B and ^{18}C . One of the targets is the $^9\text{Li} + ^9\text{Li} + n + n$ configuration of ^{20}C around the four-body threshold. The ^{11}Li nucleus is the famous halo nucleus, and how two ^9Li clusters share the two weakly bound neutrons around the threshold energy is an intriguing question. Also, we investigate the role of the cluster states obtained, including resonances above the cluster emission threshold around the

Gamow window, in the nuclear reactions including the big-bang nucleosynthesis.

ACKNOWLEDGMENTS

The authors would like to thank Dr. Masaki Sasano (RIKEN) for fruitful discussions. The numerical calculations have been performed by using the computer facility of Yukawa Institute for Theoretical Physics, Kyoto University.

-
- [1] D. M. Brink, in *Many-Body Description of Nuclear Structure and Reactions, Proceedings of the International School of Physics "Enrico Fermi", Course XXXVI, Varenna, 1965*, edited by C. Bloch (Academic, New York, 1966)
- [2] M. Freer, H. Horiuchi, Y. Kanada-En'yo, D. Lee, and U.-G. Meißner, *Rev. Mod. Phys.* **90**, 035004 (2018).
- [3] Y. Fujiwara, H. Horiuchi, K. Ikeda, M. Kamimura, K. Katō, Y. Suzuki, and E. Uegaki, *Prog. Theor. Phys. Suppl.* **68**, 29 (1980).
- [4] F. Hoyle, *Astrophys. J.* **1**, 121 (1954).
- [5] M. G. Mayer and H. G. Jensen, *Elementary Theory of Nuclear Shell Structure* (John Wiley and Sons, New York, Chapman and Hall, London, 1955).
- [6] N. Itagaki, S. Aoyama, S. Okabe, and K. Ikeda, *Phys. Rev. C* **70**, 054307 (2004).
- [7] N. Itagaki, A. V. Afanasjev, and D. Ray, *Phys. Rev. C* **101**, 034304 (2020).
- [8] N. Itagaki and S. Okabe, *Phys. Rev. C* **61**, 044306 (2000).
- [9] N. Itagaki, S. Okabe, and K. Ikeda, *Phys. Rev. C* **62**, 034301 (2000).
- [10] N. Itagaki, S. Hirose, T. Otsuka, S. Okabe, and K. Ikeda, *Phys. Rev. C* **65**, 044302 (2002).
- [11] N. Itagaki, M. Ito, M. Milin, T. Hashimoto, H. Ishiyama, and H. Miyatake, *Phys. Rev. C* **77**, 067301 (2008).
- [12] M. Ito and N. Itagaki, *Phys. Rev. C* **78**, 011602(R) (2008).
- [13] M. Ito, N. Itagaki, and K. Ikeda, *Phys. Rev. C* **85**, 014302 (2012).
- [14] P. Descouvemont and N. Itagaki, *Prog. Theor. Exp. Phys.* **2020**, 023D02 (2020).
- [15] M. Ito, N. Itagaki, H. Sakurai, and K. Ikeda, *Phys. Rev. Lett.* **100**, 182502 (2008).
- [16] M. Ito, *Phys. Rev. C* **85**, 044308 (2012).
- [17] M. Ito, *EPJ Web Conf.* **122**, 09002 (2016).
- [18] S. Aoyama, N. Itagaki, and M. Oi, *Phys. Rev. C* **74**, 017307 (2006).
- [19] N. Itagaki, M. Ito, K. Arai, S. Aoyama, and T. Kokalova, *Phys. Rev. C* **78**, 017306 (2008).
- [20] H. Esbensen and G. Bertsch, *Nucl. Phys. A* **542**, 310 (1992).
- [21] Y. Kanada-En'yo and H. Horiuchi, *Phys. Rev. C* **52**, 647 (1995).
- [22] N. Itagaki, *Phys. Rev. C* **94**, 064324 (2016).
- [23] N. Itagaki, H. Masui, M. Ito, S. Aoyama, and K. Ikeda, *Phys. Rev. C* **73**, 034310 (2006).
- [24] H. Masui and N. Itagaki, *Phys. Rev. C* **75**, 054309 (2007).
- [25] T. Yoshida, N. Itagaki, and T. Otsuka, *Phys. Rev. C* **79**, 034308 (2009).
- [26] N. Itagaki, J. Cseh, and M. Płoszajczak, *Phys. Rev. C* **83**, 014302 (2011).
- [27] T. Suhara, N. Itagaki, J. Cseh, and M. Płoszajczak, *Phys. Rev. C* **87**, 054334 (2013).
- [28] N. Itagaki, H. Matsuno, and T. Suhara, *Prog. Theor. Exp. Phys.* **2016**, 093D01 (2016).
- [29] H. Matsuno, N. Itagaki, T. Ichikawa, Y. Yoshida, and Y. Kanada-En'yo, *Prog. Theor. Exp. Phys.* **2017**, 063D01 (2017).
- [30] H. Matsuno and N. Itagaki, *Prog. Theor. Exp. Phys.* **2017**, 123D05 (2017).
- [31] N. Itagaki and A. Tohsaki, *Phys. Rev. C* **97**, 014307 (2018).
- [32] N. Itagaki, H. Matsuno, and A. Tohsaki, *Phys. Rev. C* **98**, 044306 (2018).
- [33] A. Tohsaki, *Phys. Rev. C* **49**, 1814 (1994).
- [34] R. Tamagaki, *Prog. Theor. Phys.* **39**, 91 (1968).
- [35] D. J. Marín-Lámbarri, R. Bijker, M. Freer, M. Gai, T. Kokalova, D. J. Parker, and C. Wheldon, *Phys. Rev. Lett.* **113**, 012502 (2014).